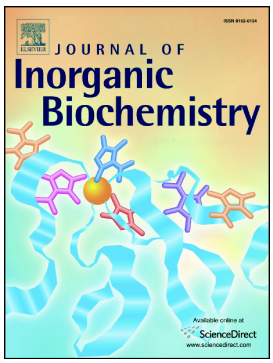

Lapachol and lawsone in the design of new ruthenium(II)-diphosphine complexes as promising anticancer metallodrugs

Katia M. Oliveira, João Honorato, Felipe C. Demidoff, Mario S. Schultz, Chaquip D. Netto, Marcia R. Cominetti, Rodrigo S. Correa, Alzir A. Batista

PII: S0162-0134(20)30317-2

DOI: https://doi.org/10.1016/j.jinorgbio.2020.111289

Reference: JIB 111289

To appear in: *Journal of Inorganic Biochemistry*

Received date: 29 July 2020

Revised date: 8 October 2020

Accepted date: 17 October 2020

Please cite this article as: K.M. Oliveira, J. Honorato, F.C. Demidoff, et al., Lapachol and lawsone in the design of new ruthenium(II)-diphosphine complexes as promising anticancer metallodrugs, *Journal of Inorganic Biochemistry* (2018), https://doi.org/10.1016/j.jinorgbio.2020.111289

Lapachol and Lawsone in the Design of New Ruthenium(II)-Diphosphine Complexes as Promising Anticancer Metallodrugs

Katia M. Oliveira[a,d,*], João Honorato[a], Felipe C. Demidoff[b], Mario S. Schultz[b], Chaquip D. Netto[b], Marcia R. Cominetti[c], Rodrigo S. Correa[d], Alzir A. Batista[a,*]

[a]*Departamento de Química, Universidade Federal de São Carlos (UFSCar), CP 676, CEP 13565-905, São Carlos - SP, Brazil*

[b]*Instituto de Química, Universidade Federal do Rio de Janeiro (UFRJ), Campus Aloísio Teixeira, CEP 27930-560, Macaé-RJ, Brazil*

[c]*Departamento de Gerontologia, Universidade Federal de São Carlos (UFSCar), CP 676, CEP 13565-905, São Carlos – SP, Brazil*

[d]*Departamento de Química, ICEB, Universidade Federal de Ouro Preto (UFOP), CEP 35400-000, Ouro Preto – MG, Brazil*

* Corresponding authors: e-mail: kmoliveiraq@gmail.com (Katia M. Oliveira) and daab@ufscar.br (Alzir A. Batista). Tel.: +55 16 33518285; Fax: +55 16 33518350.

Abstract

The development of metal complexes containing natural products is a remarkable strategy to develop new anticancer candidates. Thus, we report here on the preparation of two new Ru(II)/diphosphine complexes containing Lapachol (Lap) and Lawsone (Law): (**1**) $[Ru(Lap)(dppm)_2]PF_6$ and (**2**) $[Ru(Law)(dppm)_2]PF_6$, where dppm = *bis*(diphenylphosphino)methane. The complexes were synthetized and fully characterized by elemental analyses, molar conductivity, UV-Vis, IR, $^{31}P\{^1H\}$, ^1H and ^{13}C NMR, and the crystal structure of the complex (**1**) was determined by X-ray diffraction. Complexes (**1**) and (**2**) showed high *in vitro* cytotoxicity against four cancer cells (MDA-MB-231, MCF-7, A549 and DU-145), with IC_{50} values in the micromolar range (0.03 to 2.70 μM). Importantly, complexes (**1**) and (**2**) were more active than the cisplatin, the drug used as a reference in the cytotoxic assays. Moreover, complex (**1**) showed high selectivity to triple-negative breast

cancer cells (MDA-MB-231). Studies of the mechanism of action in MDA-MB-231 cancer cells showed that complex (**1**) inhibit cell migration, colony formation, and induces cell cycle arrest and apoptosis by activation of the mitochondrial pathway through the loss of mitochondrial membrane potential (ΔΨm). Furthermore, the complex (**1**) induces ROS generation in MDA-MB-231 cells, which can cause DNA damage. Finally, complexes (**1**) and (**2**) interact with DNA by minor grooves and show a moderate interaction with BSA, with the involvement of hydrophobic interactions. Essentially, Ru(II)/diphosphine-naphthoquinone complexes have remarkable cytotoxic effects with high selectivity to triple-negative breast cancer (MDA-MB-231) and could be promising anticancer candidates for cancer treatment.

Keywords: Ruthenium complexes, antitumor, naphthoquinones, breast cancer, apoptosis, ROS generation

Introduction

Over the last few decades, the development of anticancer agents containing metal has grown considerably, especially after the discovery of the cisplatin anticancer properties[1,2]. Since cisplatin was clinically approved for cancer treatment by the FDA in 1978, a large number of cisplatin analogs have been developed. Among them, carboplatin and oxaliplatin, have shown to be extremely successful as anticancer drugs[3–5]. Despite their effectiveness, platinum compounds showed clinical harms, as its toxicity leads to several undesired side effects, as well as provokes drug resistance. In addition, its limited solubility in aqueous solutions hampers its extensive use[6]. Thus, many research groups have focused on the development of more effective and less toxic new metal-based drugs. Within this framework, the development of new ruthenium-based compounds has emerged as a promising choice for the design of new anticancer drugs[7–11].

Ruthenium is an attractive alternative to platinum compounds due to its rich synthetic and coordination chemistry, the possibility to adopt different oxidation states, mainly II and III, in physiological conditions. Moreover, ruthenium compounds have presented distinct mechanisms of action from those of platinum, with low systemic toxicity[6,12].

The first works involving ruthenium complexes were developed by M. J. Clarke and co-workers in the 1980s, who investigated compounds such as *fac*-[$RuCl_3(NH_3)_3$] and *cis*-[$RuCl_2(NH_3)_4$]Cl[13]. After that, several reports of ruthenium complexes as anticancer agents were published[8,14]. To date, only three Ru-based compounds reached clinical trials as candidates for anticancer drugs: NAMI-A, KP1019, and NKP1339, the sodium salt analog of KP1019. NAMI-A acts as a potent antimetastatic drug, whereas KP1019 prevents the growth of platinum-resistant colorectal cancers[15]. It seems that these compounds have a multifactorial and multitarget mode of action, however their mechanism of action is still largely unclear[15]. It is also worth mentioning that the NAMI-A compound was already ruled out[16]. Furthermore, KP1019 has completed phase I trials and NPK1339 is in clinical development[17,18].

More recently, the Ru(II) polypyridyl complex called TLD-1433, entered phase II clinical trial for Non-Muscle Invasive Bladder Cancer (NMIBC), for photodynamic therapy (PDT). TLD1433 acts as a photosensitizer and produces singlet oxygen to cause cancer cell death[19,20].

The incorporation of ligands that can increase lipophilicity, and consequently, the cellular uptake and intracellular distribution is an interesting strategy for the development of potential metallodrugs. In this sense, natural products, presenting known biological activities, emerge as a promising class of compounds that can act as ligands. Recently, we have used this strategy and many classes of natural products have been chosen to obtain active ruthenium complexes[21–26].

Due to the favorable results observed for ruthenium complexes containing natural products on cancer cells, in this work, we designed new Ru(II)/diphosphine complexes containing Lapachol (Lap) and Lawsone (Law) as ligands. Lapachol (2-hydroxy-3-(3-methylbut-2-en-1-yl)naphthalene-1,4-dione) and Lawsone (2-hydroxy-1,4-naphthoquinone)

belong to the naphthoquinone class, which can be of natural or synthetic origin. These naphthoquinones exhibited antibacterial, antiparasitic and anticancer biological properties, among others[27,28].

Usually, Lap and Law can act as *O,O*-bidentate anionic ligands forming stable metal complexes. Ruthenium complexes containing these naphthoquinones showed promising activities against several cancer cell lines, confirming the synergistic effect of the combination of metal and bioactive ligand[22,23,29].

In order to investigate the influence of these naphthoquinones in a complex containing two diphosphine as ligands, we report here on the syntheses, characterization, and biological activities of two new ruthenium(II)/diphosphine-naphthoquinone complexes on different tumor and non-tumor cell lines.

Materials and methods

Materials

All reagents and chemicals used were from analytical or pure grade, and the solvents were purified based on appropriate drying agents. The synthesis was performed under inert conditions using Schlenk techniques. The $RuCl_3.nH_2O$, KPF_6, Lawsone (Law), *bis*(diphenylphosphino)methane (dppm), Calf-Thymus DNA (CT-DNA), pBR322 plasmid DNA from *E. coli*, Bovine Serum Albumin (BSA), 3-(4,5-dimethylthiazol-2-yl)-2,5-diphenyltetrazolium bromide (MTT) and 2',7'-dichlorofluorescin diacetate (H_2DCFDA) were purchased from Sigma-Aldrich® MERCK (St. Louis, MO, USA) and used as received. Lapachol (Lap) was obtained according to the procedure described in the literature[30].

Instrumentation

FT-IR spectra were acquired as KBr pellets on a Bomem-Michelson FT-MB-102 spectrophotometer, in the range of 4000 and 200 cm^{-1}. UV-Vis spectra were recorded on a Hewlett Packard diode array - 8452A spectrophotometer. Elemental analyses for C and H were determined using an CHNS Element Analyzer (Thermo Scientific, Fisons EA 1108

model). Molar conductivity was obtained using a MeterLab CDM2300 at room temperature. Electrochemical experiments were performed using a Bioanalytical Systems Inc, model BAS-100B/W at room temperature in CH_2Cl_2 containing 0.10 M of tetrabutylammonium perchlorate (Bu_4NOH). The reference electrode used was Ag/AgCl (0.10 M Bu_4NOH in CH_2Cl_2) in a Luggin capillary probe and the working and auxiliary electrodes were stationary platinum foils. $^{31}P\{^1H\}$ (162 MHz), ^1H (400 MHz) and $^{13}C\{^1H\}$ (100.62 MHz) NMR spectra were recorded on a 9.4 T Bruker Avance III 400 MHz spectrometer using a 5 mm internal diameter indirect probe with Automatic Tuning Matching.

General procedure to obtain Ru(II)/diphosphine-naphthoquinone complexes

Firstly, the precursor complex *cis*-$[RuCl_2(dppm)_2]$ was obtained according to what was described by Chatt and Sullivan[31,32]. The naphthoquinone (Lap or Law) (0.14 mmol) was added in methanol solution with 50 μL of triethylamine (Et_3N). After 30 minutes, the precursor complex *cis*-$[RuCl_2(dppm)_2]$ (0.11 mmol, 100 mg) and KPF_6 (0.21 mmol, 39 mg) were added and the reaction was kept under argon atmosphere and reflux for 18 h. Afterwards, the volume of the solution was reduced, and the precipitate formed was collected by filtration. The solid was washed with water, ethyl ether, and dried under vacuum.

(**1**) $[Ru(Lap)(dppm)_2]PF_6$. Dark green solid. Yield: 93 mg (70 %). Elemental analysis for $[RuC_{65}H_{57}F_6O_3P_5]$: exp. (calc): C, 61.74 (62.15) and H, 4.80 (4.57)%. Λ_M = 54.6 Ω^{-1} cm^2 mol^{-1}, in 1.0 mM CH_2Cl_2 solution. IR (cm^{-1}): $\nu(C_1{=}O)$ 1545, $\nu(C_4{=}O)$ 1612, $\nu(C_2{-}O)$ 1101, ν(P-F) 841 and 557, ν(Ru-N) 480 ν(Ru-O) 517. Molar extinction coefficient ($\varepsilon_{(\lambda,\ nm)}$, M^{-1} cm^{-1}): $\varepsilon_{(258\ nm)}$: 4.74×10^4, $\varepsilon_{(365\ nm)}$: 6.31×10^3, $\varepsilon_{(448\ nm)}$: 3.77×10^3, $\varepsilon_{(615\ nm)}$: 4.49×10^3. $^{31}P\{^1H\}$ NMR (162 MHz, CH_2Cl_2, 298 K): δ (ppm) 5.61 (2P, m), −10.61 and −12.42 (1P, 2m), −16.50 and −18.30 (1P, 2m), −144 (1P, hept, PF_6^-, J_{PF} = 711 Hz). ^1H NMR (400 MHz, DMSO-d_6, 298 K): δ (ppm) 7.9 – 6.3 (m, 44H, an overlap of aromatic protons of phenyl groups of dppm (20 H) and Lap (4H)), 5.4 (m, 1H, Lap), 5.2 (m, 2H, dppm), 4.2 (m, 2H, dppm), 3.2 – 3.0 (m,

2H, Lap), 1.8 – 1.6 (m, 6H, $2CH_3$ of Lap). $^{13}C\{^1H\}$ NMR (125.74 MHz, DMSO-d_6, 298 K): δ(ppm) 195.5 (C_1=O), 181.1 (C_4=O), 168.9 (C_2–O).

(**2**) [Ru(Law)(dppm)$_2$]PF_6. Dark blue solid. Yield: 97 mg (77%). Elemental analysis for [$RuC_{60}H_{49}F_6O_3P_5$]: exp. (calc): C, 61.14 (60.66), H, 4.73 (4.20)%. Λ_M = 48.2 Ω^{-1} cm^2 mol^{-1}, in 1.0 mM CH_2Cl_2 solution. IR (cm^{-1}): *ν*(C1=O) 1554, *ν*(C4=O) 1604, *ν*(C2–O) 1097, *ν*(P-F) 840 and 559, *ν*(Ru-N) 485 *ν*(Ru-O) 520. Molar extinction coefficient ($\varepsilon_{(\lambda,\ nm)}$, M^{-1} cm^{-1}): $\varepsilon_{(258\ nm)}$: 4.59 × 10^4, $\varepsilon_{(357\ nm)}$: 6.54 × 10^3, $\varepsilon_{(450\ nm)}$: 3.64 × 10^3, $\varepsilon_{(585\ nm)}$: 4.61 × 10^3. $^{31}P\{^1H\}$ NMR (162 MHz, CH_2Cl_2, 298 K): δ (ppm) 5.93 (2P, m), –11.17 and –15.02 (1P, 2m), –15.39 and –17.17 (1P, 2m), –144 (1P, hept, PF_6^-, J_{PF} = 711 Hz). ^1H NMR (400 MHz, DMSO-d_6, 298 K): δ (ppm) 7.8 – 6.3 (m, 44H, an overlap of aromatic protons of phenyl groups of dppm (20 H) and Law (4H), 5.90 (s, 1H, Law), 5.4 – 5.0 (m, 2H, dppm), 4.2 – 4.1 (m, 2H, dppm); $^{13}C\{^1H\}$ NMR (125.74 MHz, DMSO-d_6, 298 K): δ (ppm) 196.20 (C_1=O), 182.24 (C_4=O) and 171.54 (C_2□O).

X-ray crystallography

Green single crystal of complex (**1**) was obtained from slow evaporation of a dichloromethane/ethyl ether solution. Room temperature X-ray crystallographic analysis was carried out using an automatic Rigaku XtaLAB mini II diffractometer (graphite monochromator) with Mo-Kα radiation (λ = 0.71073 Å), in which intensities were collected (ω scans with θ and κ-offsets), integrated and scaled with CrysAlisPro[33]. The structure was solved by the direct method using SHELXS-97 and refined using the software SHELXL-97[34]. All non-hydrogen atoms of the complex, counter-ion and solvent were located and refined with anisotropic thermal parameters. The hydrogen atoms of aromatic C–H and CH_2 methylene groups of dichloromethane, dppm and lapachol were positioned and refined with fixed displacement parameters [Uiso(H) = 1.2 Ueq(Csp^2)] using a riding model with bond lengths of 0.93 and 0.97 Å, respectively. Finally, C-H of methyl were located from an

electron-density difference and refined as riding on their parent atoms with $U_{iso}(H)$ values of $1.5U_{eq}(Csp^3)$ and C-H distance of 0.96 Å Molecular representations were generated using the MERCURY 4.0[35] program. The summary of crystal data collections and structure refinement parameters are presented in Table S1 (supplementary information) and copies of the data can be obtained, free of charge, on the CCDC (Cambridge Crystallographic Data Centre) under deposition number 2003981.

DNA interaction studies

***Agarose gel electrophoresis*.** The pBR322 DNA (35 μM) was mixed with the ruthenium complexes in different molar ratios ([complexes]/[DNA]): 0.05 to 2) and the solutions were incubated for 18 h at 37 °C. The samples were electrophoresed in agarose gel using a Tris-acetate-EDTA buffer (0.45 M Tris-HCl, 0.45 M acetic acid, 10 mM EDTA, pH 7.4). Ethidium bromide was used for staining. The bands were visualized and registered using a ChemiDoc MP imager (BioRad Laboratories, Hercules, CA, USA).

Circular Dichroism. Circular Dichroism (CD) spectrum of CT-DNA was obtained from the CT-DNA solution prepared in a Tris-HCl buffer (4.5 mM Tris-HCl, 0.5 mM Tris-base and 50 mM NaCl, pH = 7.4). The experiment was performed by keeping the CT-DNA concentration constant at 50 μM and varying the concentration of the ruthenium complexes to obtain the molar ratios ([complexes]/[DNA]) of 0.05 to 0.4. The samples were prepared in a Tris-HCl buffer containing 10% of DMSO, and incubated for 18h at 37 °C. The CD spectra were recorded using a spectropolarimeter JASCO J720 in the range of 240 to 350 nm at 298 K, with a constant nitrogen flush. Each spectrum was performed using a circular quartz cuvette with 1cm path length.

***Competitive DNA-Hoechst assay*.** The Hoechst 33258 fluorophore can intercalate the minor grooves of CT-DNA and shows an emission spectrum at 475 nm. The experiment was conducted using a Hoechst solution (2.7 μM) and CT-DNA (125 μM), which was titrated

with an increasing amounts of ruthenium complexes (0 – 100 μM) in Tris-HCl buffer containing 10% DMSO. The fluorescence spectra were registered in the range of 370 to 700 nm with an excitation wavelength of 343 nm using a Synergy/H1-Biotek fluorimeter at 37 °C.

Protein binding studies

The protein binding studies were performed by fluorescence quenching using Bovine Serum Albumin (BSA, 2.5 μM) in a Tris-HCl buffer. The stock solutions of the ruthenium complexes were prepared in DMSO, and then incubated with BSA in different concentrations (0 - 90 μM). The fluorescence spectra were recorded at 298 and 310 K, with and excitation wavelength of BSA at λ_{ex} = 280 nm and emission at λ_{em} = 340 nm, using a fluorimeter SpectraMax M3. The analyses were carried out in triplicate and the results were analyzed using the Stern-Volmer Equation[36]:

$$F_0/F = 1+ k_q\tau_0[Q] = 1 + K_{sv}[Q] \quad \textbf{(1)}$$

where F_0 and F are the fluorescence intensity of BSA in the absence and presence of complexes, respectively, K_{sv} is the Stern-Volmer constant, [Q] is the concentration of complexes, k_q is the biomolecular quenching constant and τ_0 is the average lifetime of BSA without the quencher (~ 10^{-8} s)[36].

The binding constant (K_b) and number of binding site (*n*) were obtained using equation (2)[36]:

$$\log[(F_0\text{-}F)/F] = \log K_b + n\log[Q] \quad \textbf{(2)}$$

Additionally, thermodynamic parameters such as enthalpy (ΔH°), entropy (ΔS°) and Gibbs energy (ΔG°) were determined, using equations (3) and (4)[37]:

$$\ln(K_{b1}/K_{b2}) = (1/T_1 - 1/T_2) \times \Delta H/R \quad \textbf{(3)}$$

$$\Delta G° = - RT\ln K_b = \Delta H° - T\Delta S° \quad \textbf{(4)}$$

MTT assay

The effects of the ruthenium complexes, the ligands Lapachol, Lawsone and the cisplatin on the cell lines viability were determined by the MTT (3-(4,5-dimethylthiazol-2-yl)-2,5-diphenyltetrazolium bromide) assay[38].

The cell lines were the human breast MCF-7 (ATCC: HTB-22) and MDA-MB-231 (ATCC: HTB-26), human prostate DU-145 (ATCC: HTB-81), human lung A549 (ATCC: CCL-185) and non-tumor breast cells, MCF-10A (ATCC: CRL-10317). The MDA-MB-231 and A549 cells were routinely grown in Dulbecco's modified Eagle's medium (DMEM) supplemented with 10% FBS. MCF-7 and DU-145 cells were cultivated in Roswell Park Memorial Institute medium (RPMI-1640) supplemented with 10% fetal bovine serum (FBS). MCF-10A cells were maintained in DMEM/F12 medium containing horse serum (HS) 5%, EGF (0.02 mg mL^{-1}), hydrocortisone (0.05 mg mL^{-1}) and insulin (0.01 mg mL^{-1}). All the media contained penicillin (100 UI mL^{-1}), streptomycin (100 mg mL^{-1}) and L-glutamine (2 mM).

MDA-MB-231, MCF-7, A549, DU-145 and MCF-10A cells (1.5×10^4 cells/well) were seeded in 96-well plates in 100 μL of media and were allowed to attach overnight in a CO_2 incubator at 37 ºC. The compounds were added in different concentrations in triplicate and incubated for 48 h. The percentage of DMSO used in the experiments was fixed at 0.5%. The control cells were treated only with 0.5% of DMSO. Afterwards, 40 μL of MTT (1 mg mL^{-1}) solution was added to each well and the plates were incubated for 4 h at 37 °C. Finally, 100 μL of isopropanol was added to each well to dissolve the purple formazan crystals. The absorbance at 540 nm was determined using a microplate reader (Bio-Tek instruments). The IC_{50} values were determined using the GraphPad Prism software.

Morphology assay

MDA-MB-231 and MCF-10A cells (1×10^5 cells/well) were seeded in 12-well plates and incubated for approximately 24 h in a CO_2 incubator at 37 °C. After that, the complex (**1**)

was added in different concentrations (0.01 to 15 μM). Cells were examined using an inverted optical microscope (Nikon, T5100) with an amplification of 100×. Images of cell morphology were recorded at 0, 24 and 48 h of incubation with ruthenium complex. Control cells were treated with 0.5 % DMSO.

Colony formation assay

MDA-MB-231 (300 cells/plate) were seeded into 6 cm Petri dishes and incubated for approximately 24 h in a CO_2 incubator at 37 °C. Complex (**1**) was added in different concentrations (0.03 to 1 μM) and incubated for 48 h. Next, the medium was removed and a fresh medium without complex was added and cells were incubated for 10 days. Afterwards, cells were fixed using methanol and acetic acid (3:1) for 15 min and stained with crystal violet solution (1% crystal violet, 20% ethanol) for 30 min. The plates were washed in water to remove extra dye. The colonies (> 50 cells) were quantified and measured using ImageJ Software.

Wound healing assay

To evaluate the ability of complex (**1**) to inhibit cell migration, MDA-MB-231 cells (1×10^5 cells/wells) were seeded in 12-well plates and incubated at 37 ºC in 5% CO_2 up to 80% of confluence. A straight scratch was performed on the plate using a sterile pipette tip. The removed cells were washed to eliminate debris and a new medium with different concentrations of complex (**1**) (0.1, 0.5 and 1 μM) was added. Migrating cells were photographed using an inverted microscope at 0, 8 and 24 h. The closure area of migrating cells was quantified using ImageJ software, as follows: Wound healing area (%) = [cell-free area (0 h) – cell-free area (24 h)]/cell-free area (0 h) × 100.

Cell migration assay

MDA-MB-231 cells (0.5×10^5 cells/well) in serum-free medium were seeded on the upper chamber of Boyden transwell chambers. Complex (**1**) was added in different concentrations, below the IC_{50} for cytotoxic assay after 24 h (0.1, 0.5 and 1 μM). Medium with 10% of FBS was added to the bottom chamber to act as a chemoattractant in the positive control of migration. For the negative control of cell migration, serum-free medium was added to the lower chamber. The transwell chambers were incubated at 37 °C and 5% CO_2 for 24 h. After that, the cells that migrated were fixed with methanol for 10 min, stained with toluidine blue, and washed with distilled water. Images of the membrane were registered using an inverted microscope (Nikon Eclipe TS100) coupled to a camera (Moticam 1000 - 1.3MP Live Resolution), and the migrated cells were quantified using ImageJ software. The data shows the mean of cells that migrated in two independent experiments ± SD.

Cell death analysis

Apoptosis/necrosis of cells treated with complex (**1**) was investigated using 7-AAD annexin V and PE (BD Biosciences) staining. MDA-MB-231 cells (0.7×10^5 cells/well) were plated in 24-well plates, and after 24 h of incubation at 37 °C and 5% CO_2 were exposed to different concentrations of complex (1) (0.5 to 10 μM) and incubated again for 24 h. Thereafter, the cells were stained with 2.5 μL of PE-Annexin-V and 2.5 μL of 7-AAD, in the dark for 15 min, according to the manufacturer's directions. Analyses were performed using a flow cytometer BD Accurri C6 Plus.

Cell cycle analysis

MDA-MB-231 cells (1×10^5 cells/well) were seeded in 12-well plates and incubated overnight at 37 °C and 5% CO_2. Then, different concentrations of complex (**1**) (0.1 to 1.25 μM) were added to the cells and incubated for 24 h. After the incubation period, the cells were collected and fixed with 70% cold ethanol for 24 h. Posteriorly, the cells were

centrifuged and incubated with 300 μL of RNase A (0.2 mg mL^{-1}) for 30 min at 37 °C. Cells were stained using hypothonic fluorochrome solution (propidium iodide 5 μg mL^{-1}, sodium citrate 0.1% and Triton-X-100 0.1%) for 1 h. The samples were analyzed using a Biosciences Accuri C6 BD, and 10,000 cells were counted in each sample. This assay was performed in triplicate and the data were processed using C6 Plus Software.

Reactive oxygen species

The levels of intracellular ROS generation in MDA-MB-231 cells induced by complex (**1**) were measured using H_2DCFDA (2',7'-dichlorofluorescin diacetate). To do this, MDA-MB-231 cells (6×10^5 cells/well) were seeded into 6-well plates and incubated overnight at 37 °C and 5% CO_2. Then, the cells were treated with complex (**1**) ($3 \times IC_{50}$ of 24h) and with free Lap (10 μM), for 4 h. H_2O_2 (10 μM) was used as the positive control and as negative control, cells containing only 0.5% of DMSO. Next, cells were washed with PBS and incubated with 10 μM of H_2DCFDA for 30 min at 37 °C. Cells were washed using ice-cold PBS (3×) and harvested. The fluorescence analysis was carried out using a Synergy H1 Hybrid Multi-Mode Microplate Fluorimeter at a λ_{ex} = 400 nm and λ_{em} = 525 nm. Images were registered using an Olympus BX50 fluorescence microscope.

Mitochondrial membrane potential

Changes in the mitochondrial potential (ΔΨm) of MDA-MB-231 cells after treatment with complex (**1**) were investigated using a DBTM MitoScreen Kit with JC-1 (5',5',6,6'-tetrachloro-1,1',3,3' tetraethylbenzimidazolcarbocyanine iodide) dye. Briefly, MDA-MB-231 cells (1×10^5) were seeded in 12-well plates and incubated overnight to allow cells to attach prior to adding complex (**1**) at different concentrations (IC_{50} of 24 h and $2\times$ IC_{50} of 24 h), followed for additional incubation for 4 h. Cells were washed in ice-cold PBS, stained with JC-1 in the dark, according to the manufacturer's directions and the samples were analyzed using a BD Accurri C6 Plus flow cytometer.

Results and Discussion

Synthesis and Characterization

Ruthenium-naphthoquinone complexes identified as: (**1**) $[Ru(Lap)(dppm)_2]PF_6$ and (**2**) $[Ru(Law)(dppm)_2]PF_6$ [Lap = Lapachol, Law = Lawsone and dppm = *bis*(diphenylphosphine)methane)], were obtained from the precursor complex *cis*-$[RuCl_2(dppm)_2]$, by substituting two chloride ligands and coordination of Lap or Law after deprotonation with triethylamine (Et_3N), in methanol media (Scheme 1).

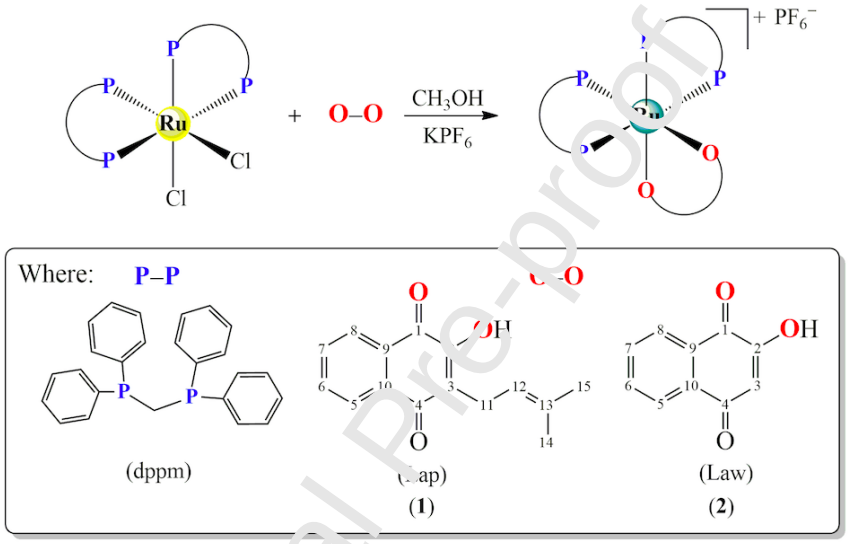

Scheme 1. Synthetic route used to obtain complexes (**1**) $[Ru(Lap)(dppm)_2]PF_6$ and (**2**) $[Ru(Law)(dppm)_2]PF_6$.

Both complexes (**1**) and (**2**) were obtained as an air-stable solid, soluble in solvents such as methanol, ethanol, dichloromethane, acetone and DMSO. On the other hand, the compounds are insoluble in water, ethyl ether and hexane. The percentages of C and H obtained by elemental analysis agree with the theoretical values. Moreover, the molar conductivity result indicates that the complexes are cationic, with the PF_6^- as an anion.

The IR spectrum of the free Lap/Law show bands around 3354, 1643 and 1050 cm^{-1}, assigned to *ν*(O-H), *ν*(C1=O) and *ν*(C2-O), stretching vibrations, respectively. Upon coordination of Lap or Law, the band assigned to the *ν*(O-H) stretching vibration was not observed, indicating the deprotonation and coordination by the oxygen as monoanionic. Moreover, the *ν*(C1=O) and *ν*(C2-O) bands were shifted after coordination (Fig S1 and S2).

For complex (**1**), these bands were observed at 1545 (C1=O) and 1101 (C2-O) cm^{-1}, indicating the bidentate coordination of Lap by oxygen atoms[23]. In addition to those bands, it was observed characteristic bands of a PF_6^- counterion were observed at 841 and 557 cm^{-1}, which are in agreement with molar conductance, consistent with 1:1 electrolyte. For complexes (**1**) and (**2**) containing the dppm, weak band corresponding to ν(P-CH_2) at around 660 cm^{-1} was observed. Moreover, ν(Ru-O) and ν(Ru-N) were observed at 480 and 520 cm^{-1}, respectively[39].

The electronic spectra of complexes (**1**) and (**2**) presented characteristic bands of intraligand transitions IL ($\pi \rightarrow \pi^*$) around 260 and 290 nm of the dppm and Lap/Law ligands. In addition, bands around 400 and 600 nm can be assigned to metal-to-ligands charge transfer (MLCT), from Ru(dπ) to the ligand (π^*) and also, $n \rightarrow \pi^*$ transitions of quinone carbonyl groups (Fig S3)[21–23].

The electrochemical behavior of complexes (**1**) and (**2**) have been studied in CH_2Cl_2 by cyclic voltammetry. This study is useful to determine the changes in the electronic density of ruthenium(II) upon coordination of Lap or Law. The precursor complex *cis*-[$RuCl_2(dppm)_2$] exhibits an oxidation process referring to Ru^{II}/Ru^{III} at 1043 mV. After the coordination of Lap or Law, the oxidation processes Ru^{II}/Ru^{III} increased considerably (Fig. S4-S5). For complex (**1**) it was observed a positive shift of potential for Ru^{II}/Ru^{III} couple after coordination of Lap to 1373 mV, while in complex (**2**) the potential presents the value of 1435 mV. The presence of the prenyl group in the lapachol molecule can contribute to electron donation to ruthenium, justifying the lower potential of complex (**1**) compared to complex (**2**). In addition, the higher oxidation potentials observed for complexes (**1**) and (**2**) compared with the precursor are due to the replacement of two chloride ligands, which are good donors of electronic density by oxygen atoms, poor donors. These results confirm a greater stability of both complexes after the coordination of the Lap or Law ligands. The same

behavior was observed for complexes containing Lap or Law, in the previous work of our research group[23].

The $^{31}P\{^{1}H\}$ NMR spectra of complexes (**1**) and (**2**) showed a typical ABMX spin system. For complex (**1**), a set of signals in the region of −10.61, −12.42, −16.50 and −18.30 ppm is equivalent to the two phosphorus *trans* positioned to the two other phosphorus atoms. In 5.61 ppm, a multiplet is observed that refers to the two phosphorus *trans* positioned to the oxygen atoms of the Lap (Fig. S6). Complexes (**1**) and (**2**) showed downfield shifts in positions of the phosphorus signals as compared to the precursor complex (*cis*-$[RuCl_2(dppm)_2]$: δ −0.65 and −26.17 ppm ($^{3}J_{P\text{-}P}$ = 35.6 Hz). This is attributed to the exchange of two chlorido ligands (σ and π-donor) and coordination of Lap or Law to the ruthenium by oxygens that unshielded the phosphorus atoms. The same behavior was observed for the ruthenium complex containing mercaptopyrimidine as ligands, observed in earlier studies[40]. Furthermore, a septet around -144 ppm due to the PF_6^- anion was observed confirming the presence of the counterion in complexes (**1**) and (**2**).

^{1}H and ^{13}C NMR spectra of complexes (**1**) and (**2**) exhibited signals consistent with the structures proposed by other techniques (Fig. S7 – S11). The ^{1}H NMR spectrum of complex (**1**), for example, showed a set of signs in the region of 7.87 to 6.33 ppm, which are equivalent to 44H of the aromatic groups of dppm and Lap ligands. Signals referring to six hydrogen atoms of the two CH_3 groups of Lap were observed at 1.76 – 1.61 ppm (Fig. S7). Furthermore, the most informative result provided by the ^{13}C NMR spectra of complexes (**1**) and (**2**) are related to the C_1=O and C_2–O carbon atoms. These signals were observed around 195.5 (C_1=O) and 168.9 (C_2–O) ppm, in complex (**1**). On the other hand, in the free Lap, these signals are observed at around 184.8 (C_1=O) and 152.9 (C_2–O) ppm. The displacement can be attributed to the effect of the coordination of oxygen atoms to the metal, changing the electronic density.

The molecular structure of complex (**1**) was obtained by single-crystal X-ray crystallography (Figure 1). Complex (**1**) crystallizes in the non-centrosymmetric monoclinic Pn space group, with lattice parameters: a = 15.2069(3) Å; b = 12.0838(2) Å; c = 16.9390(3) Å; β = 93.999(2)°; Z = 2, in which the asymmetric unit consists of one molecule of cationic complex, one counterion PF_6^- and one dichloromethane as solvate (Table S1). As previously confirmed by the other characterizations, the structure of complex (**1**) is stabilized by three chelate ligands, with two dppm forming a tensioned four-membered ring [with P-Ru-P chelate bite angle of 71.40(5) - 71.66(5)°] and lapachol with a five-membered assuming a bite angle of 75.50(14)°. The structure of complex (**1**) presents a distorted octahedral geometry, which is comparable with other ruthenium/phosphine analogs with lapachol[21,23,41]. Analyzing the bond lengths, the Ru1-O1 [2.139(4) Å] and Ru1-C2 [2.136(4) Å] bonds are quite similar because both oxygen atoms are *trans* to phosphorus of dppm. Similarly, due to the same stereochemistry, the Ru-P1 [2.2967(14) Å] and Ru-P3 [2.3028(13) Å] separation is close, while Ru-P2 [2.3649(13) Å] and Ru-P4 [2.3439(14) Å] distances present almost the same values. As can be seen, both Ru-P2 and Ru-P4 lengths are larger than the Ru-P1/Ru-P3 separation, because of higher *trans* influence when phosphorus is *trans* to phosphorus, compared with phosphorus is *trans* to oxygen[42].

The lapachol molecule coordinated to metal is composed by a naphthoquinone ring almost planar and one no coplanar prenyl chain. The C-O bonds occurring in the lapachol free of metal present the values of 1.226(2), 1.348(2), and 1.225(2) Å for C1-O1, C2-O2, and C4-O4, respectively[43]. After coordination, the C1-O1, C2-O2, and C4-O4 distances adopt the values of 1.234(7), 1.295(7), and 1.233(8) Å, respectively, in which the main change is observed for the C2-O2 bond length that is slightly shortened as a result of deprotonation and coordination.

A detailed analysis of intermolecular contacts of the molecule was carried out. The molecule is well-ordered by hydrophobic regions formed mainly by C-H of diphosphines and prenyl able to be involved in van der Waals contacts (Figure S12A). Only around the C4-O4 carbonyl group displays capability to form polar contacts, such as hydrogen bonds with macromolecules[44,45]. Besides van der Waals contacts, the crystal packing is stabilized by weak hydrogen bonds connecting the complex/counter-ion and complex/solvent (Figure S12B). These intermolecular interactions display an important role to stabilize the molecular conformation and crystal self-assembly of Ru(II)-based complexes[46]. In the complex (**1**), intermolecular interactions involving the O4 atom C1s-H1sa of the (CH_2) group of the solvent and C413-H413…Cl2s present the separation of 2.521 Å and 2.774 Å, respectively. Moreover, one interaction between C1s-H1sb of solvent and F5 atom of counter-ion [distance of 2.474 Å] contributes to keep the guest solvent caged.

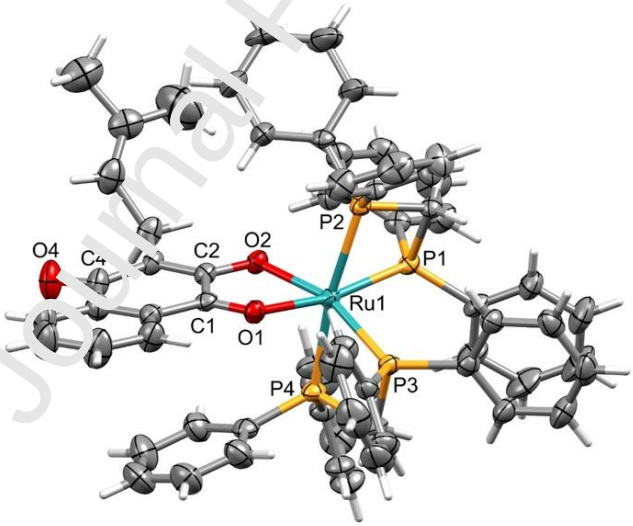

Figure 1. Crystal structure representation of the complex (**1**) at 30% probability thermal ellipsoids. For the sake of clarity, the molecules of PF_6^- and CH_2Cl_2 were omitted.

Biological investigation

Cytotoxicity assay

The cytotoxic effects of ruthenium complexes (**1**) and (**2**) were evaluated by MTT assay against four cancerous cell lines, including triple-negative breast (MDA-MB-231),

hormone-dependent breast (MCF-7), lung (A549) and prostate (DU-145). Moreover, one non-tumor cell line from the epithelial breast tissue was tested, (MCF-10A). The IC_{50} and selective index (SI) for complexes (**1**), (**2**), precursor complex *cis*-[$RuCl_2(dppm)_2$] and cisplatin, after 48 h of incubation, are summarized in Table 1. All ruthenium complexes showed cytotoxicity activity with IC_{50} values lower than those of cisplatin and the free ligands Lap and Law. In general, the cytotoxicity of the complex containing Lap (**1**) and Law (**2**) was similar. Although the IC_{50} values of complexes (**1**) and (**2**) and complex precursor are close, one interesting observation refers to the high selectivity (20 times more active) of complex (**1**) to the triple-negative breast cancer (MDA MB-231) compared to non-tumor breast cells (MCF-10A). This result confirms that the coordination of the Lap or Law to ruthenium, forming (**1**) and (**2**), increase the cytotoxicity effect and their selectivity. Moreover, complex (**1**) was 27-fold cytotoxic than cisplatin against MDA-MB-231 cells. Complexes (**1**) and (**2**) showed similar or better cytotoxic activity than complexes previously reported by our research group[23].

Given that complex (**1**) showed high selectivity for tumor MDA-MB-231 cells, it was selected for further investigations related to better understanding its mechanism of action. It is worth mentioning that before carrying out biological experiments, the stability of complex (**1**) in DMSO was studied using the $^{31}P\{^1H\}$ NMR assay, and it was observed that the complex is stable in this solvent after 72 h (Fig. S13).

Table 1. IC_{50} (μM) values of ruthenium complexes and cisplatin, toward tumor and non-tumor cell lines

Compounds	IC_{50} (μM); 48 h				
	(**1**)	(**2**)	*(**a**)	Cisplatin	Lap and Law
A549	(0.063 ± 0.018)	(0.03 ± 0.01)	(0.35 ± 0.07)	(11.54 ± 1.19)	>100
DU-145	(0.11 ± 0.05)	(0.06 ± 0.02)	(1.17 ± 0.01)	(2.00 ± 0.47)	>100
MCF-7	(2.03 ± 0.26)	(1.15 ± 0.19)	(1.17 ± 0.21)	(13.98 ± 2.02)	>100
MDA-MB-231	(0.13 ± 0.01)	(0.09 ± 0.02)	(1.10 ± 0.09)	(2.43 ± 0.20)	>100

MCF-10A	(2.70 ± 0.50)	(0.55 ± 0.07)	(3.11 ± 0.04)	(29.45 ± 0.85)	>100
$^{\#}SI^{1}$	1.33	0.48	2.66	2.11	--
$^{\#}SI^{2}$	20.77	6.11	2.88	12.12	--

*_cis_-[$RuCl_2(dppm)_2$], $^{\#}$SI = Selectivity Index = SI^1 = IC_{50}MCF-10A/IC_{50}MCF-7 e SI^2 = IC_{50} MCF-10A/IC_{50} MDA-MB-231

The MDA-MB-231 and MCF-10A cells were incubated with complex (**1**) in different concentrations and changes in the morphology of these cells have been recorded over time (Figure 2). After 48 h of incubation, MDA-MB-231 and MCF-10A cells treated with 0.13 μM and 2.7 μM (IC_{50} concentration), respectively, showed alterations in the morphology and a reduced cell number. At 5 and 15 μM, morphology of tumor cells has been completely changed, exhibiting loss of adhesion, shrinkage and fragmentation. On the other hand, in the non-tumor cells these morphological changes were subtler and only pronounced when complex (**1**) was incubated at 15 μM for 24 and 48 h. These observations are in accordance with the results of cytotoxicity activity and corroborate with the higher selectivity of complex (**1**) to MDA-MB-231 cells.

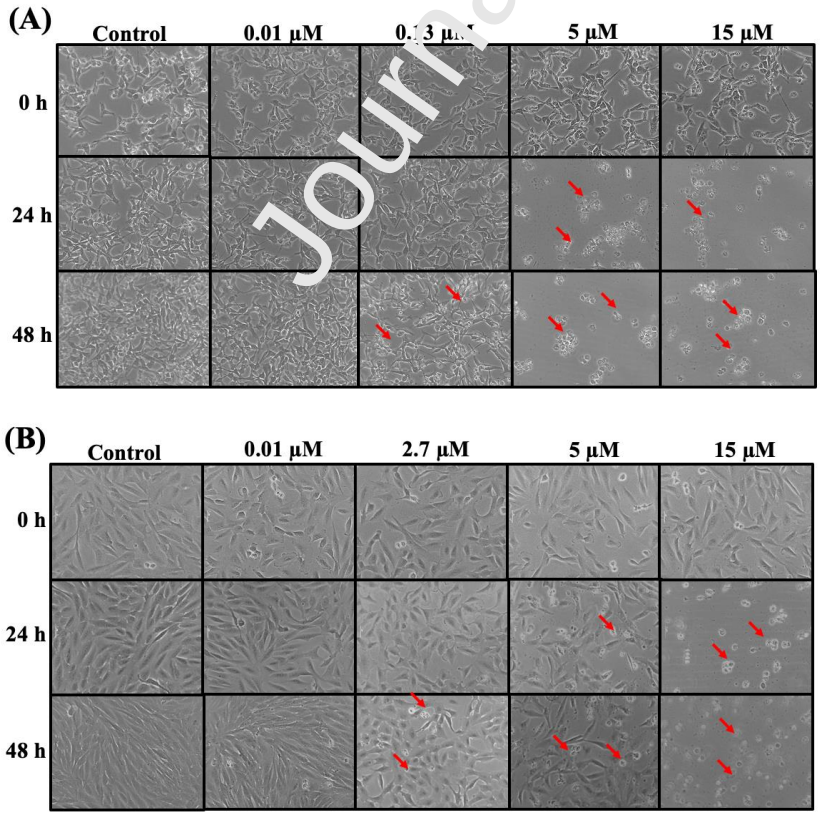

Figure 2. Effects of complex (**1**) on cell morphology of (**A**) MDA-MB-231 and (**B**) MCF-10A cells, after exposure of 0, 24 and 48 h.

The ability of a single cell to grow in a colony, after being exposed to complex (**1**), was investigated based on the clonogenic assay. The cells exposed to 0.13 (IC_{50} concentration), 0.3 and 1 μM demonstrated a significant decrease in the number and size of colonies, when compared to the negative control (Figure 3). In fact, at 0.3 and 1 μM was not possible to observe colony formation.

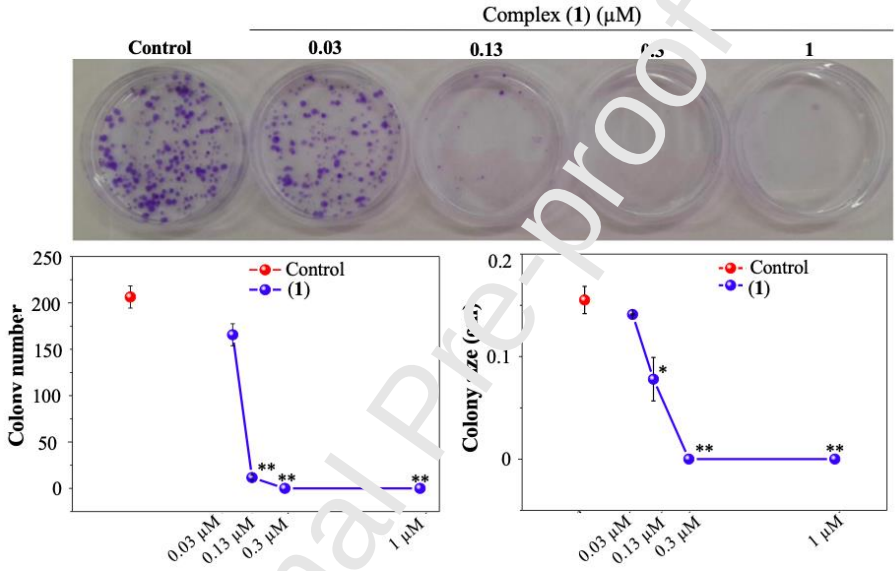

Figure 3. Representative images of clonogenic assay showing MDA-MB-231 cells treated with complex (**1**) and graphs of quantifications of colony number and size. These experiments were representative of three independent assays. Significance at the * $p < 0.01$ and ** $p < 0.0001$ using ANOVA followed by Tukey's test.

Metastatic dissemination gives rise to new tumors in other regions of the body. Briefly, this process involves different steps, such as migration, invasion, transport through the circulatory system, and growth into a secondary organ. Metastases are responsible for 90% of the deaths, and for this reason, it is important to control this process, to ensure an effective cancer treatment[47]. Herein, we evaluated the effects of complex (**1**) on the migration of MDA-MB-231 cells, which are known for their notable invasive properties. To do this, the wound healing and transwell assays were used. Complex (**1**) was capable to

inhibit cell migration at concentrations of 0.5 and 1 μM after 24 h of incubation (Figure 4 A). The wound closure reduced from 73% to 19%, for control and complex (**1**) at 1 μM, respectively. Furthermore, we also investigated the ability of complex (**1**) inhibit the cell migration through the basement membrane (physical barrier) using a Boyden-Chamber assay. After 24 h of incubation, complex (**1**) effectively inhibited the cell migration (Figure 4 B) at 0.5 and 1 μM, concentrations that are lower than IC_{50} at 24 h (IC_{50} = 1.27 ± 0.10 μM), when compared to the control. This is in accordance with wound-healing results, and clearly confirms that complex (**1**) is capable of acting as an inhibitor of cell migration at non-cytotoxic concentrations.

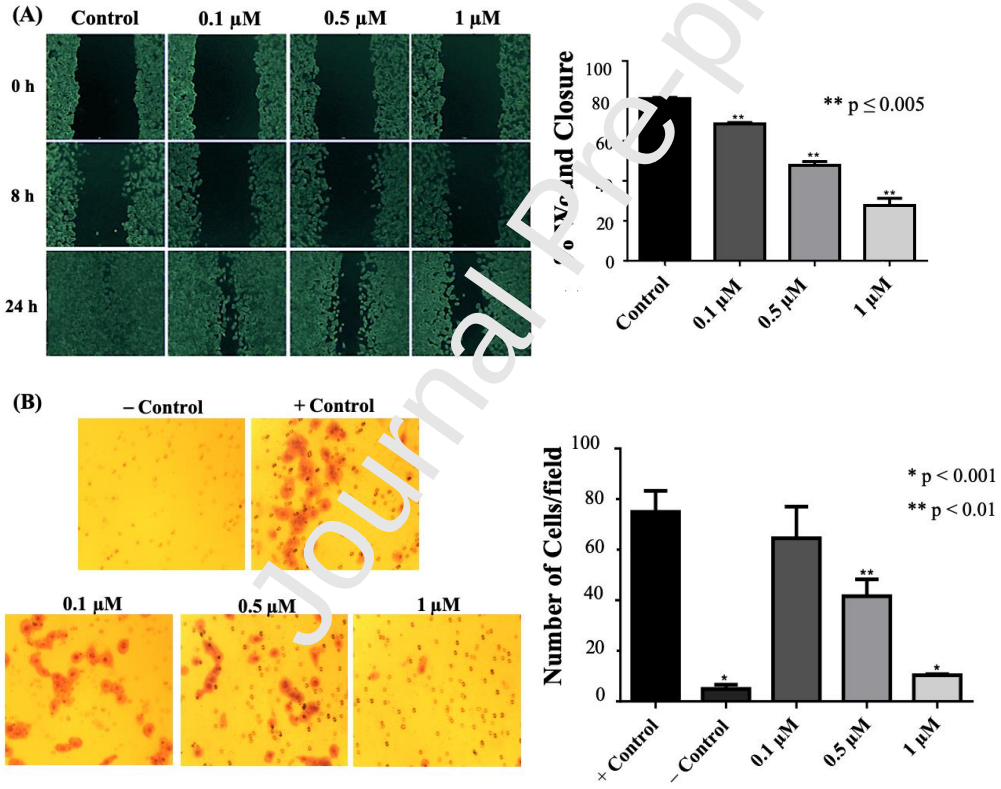

Figure 4. Effects of complex (**1**) on MDA-MB-231 cell migration. (**A**) Representative images of cells after treatment with the indicated concentrations of complex (**1**) taken at 0, 8 and 24 h using an inverted microscope (4×). (**B**) Quantitative analysis of the cell migration after treatment with the indicated concentrations of complex (**1**), by measuring the cell wounded region using ImageJ software. (**C**) Representative images of cell migration through the membranes examined using Boyden Chambers by using the inverted microscope (10×). (**D**) Percentage of migrating cells after 24 h of incubation with complex (**1**). Values were

expressed as means ± SD in triplicates. Significance at the indicated p, using ANOVA followed by the Tukey's test.

The effects of complex (**1**) on the cell cycle distribution were evaluated in MDA-MB-231 cells using flow cytometry analysis. To do this, the cells were exposed to complex (**1**) in different concentrations (0.1, 0.5 and 1.25 µM) for 24 h. Complex (**1**) caused alterations in cell cycle distribution with increased percentage of cells at Sub-G1 and G1 phases, whereas this percentage decreased at S and G2 phases (Fig. S14). The increase in cells at the Sub-G1 phase is an indicative of apoptosis[48].

To prove that this type of cell death occurs when MDA MB-231 cells were treated with different concentrations (0.5 – 10 µM) of complex (**1**), flow cytometry analysis using PE-Annexin-V and 7- AAD detection kit was performed. The percentage of apoptotic cells increases considerably with an increase of the concentration of the complex (**1**), compared to untreated control (Figure 5). The percentage of cells in apoptosis was 23.2% and 86.2%, when incubated with 1.25 µM (IC_{50} at 24 h = 1.27 ± 0.10 µM) and 10 µM, respectively, showing that the complex (**1**) induces tumor cell death via an apoptotic pathway.

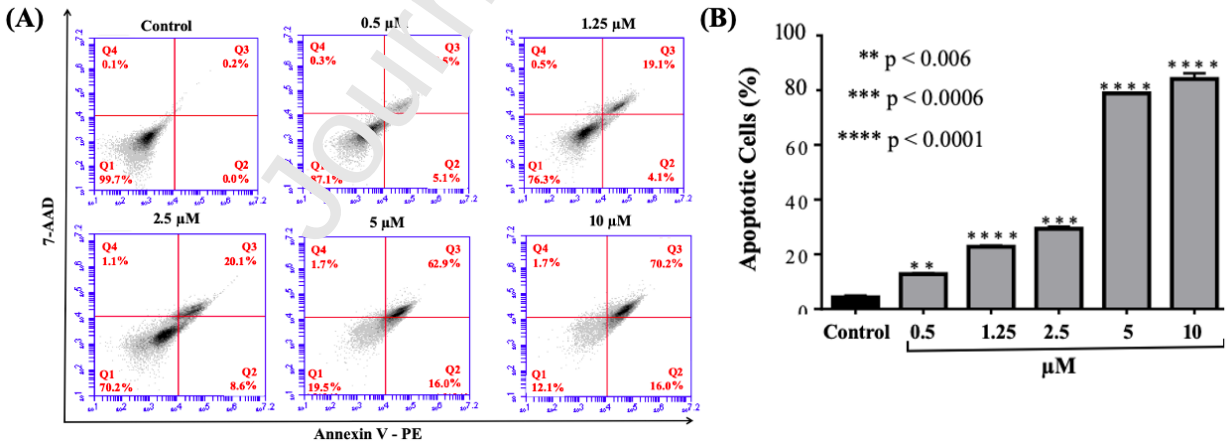

Figure 5. Effects of complex (**1**) on MDA-MB-231 cell apoptosis. (**A**) Representative overlay dot plot from apoptosis analysis of MDA-MB-231 cell after treatment with complex (**1**) for 24 h by flow cytometry using annexin V-PE vs 7AAD staining. (**B**) Quantitative analysis of apoptotic cells after treatment with the indicated concentrations of complex (**1**).

Data are represented as mean ± SD of three replicates. Significance at the indicated p, using ANOVA followed by Tukey's test.

Mitochondrial membrane potential

Mitochondria is an important organelle in cellular metabolism and is able to activate the extrinsic and intrinsic apoptotic pathways[49], acting as a target for cell death. Compounds that have mitochondria as targets are promising in anticancer drug development. The mitochondrial membrane potential (ΔΨm) is an indicator of the its regulation[50].

An important probe used to investigate the ΔΨm is JC-1, which exhibits a red fluorescence in normal conditions of mitochondria, and green fluorescence when this organelle is perturbed[51].

As shown in Figure 6, a considerable increase in bright green fluorescence (R2) indicates the loss of ΔΨm induced by complex (1), suggesting that this complex promotes mitochondrial dysfunction probably leading to cell apoptosis.

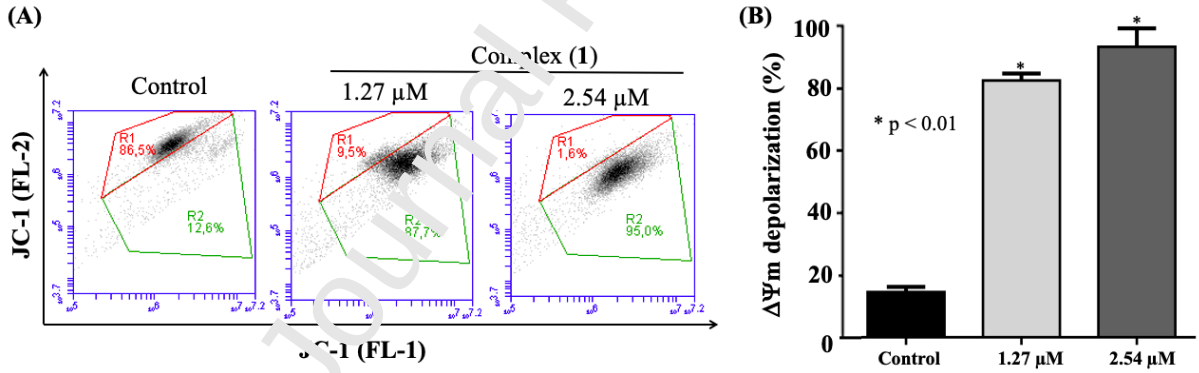

Figure 6. Effects of complex (**1**) on the ΔΨm of MDA-MB-231 cells. (**A**) Analysis of the ΔΨm of MDA-MB-231 cells after 4h of treatment with complex (**1**) at 1.27 and 2.54 µM by flow cytometry. (**B**) Quantitative analysis of the ΔΨm of MDA-MB-231 cells. Data are represented as mean ± SD of three replicates. Significance at the indicated p, using ANOVA followed by Tukey's test.

Reactive Oxygen Species (ROS)

Several studies have shown that the cytotoxic effects of naphthoquinones are mediated via ROS generation[52]. ROS can be responsible for many physiological processes, for example, activating tyrosine kinases and acting as mediators in signal transduction.

Nevertheless, ROS can also induce oxidative stress and trigger the activation of apoptotic cell signaling[53,54].

Thus, experiments were performed to determine whether complex (**1**) can generate ROS in MDA-MB-231 cells. The analysis was carried out monitoring intracellular ROS levels using H_2DCFDA (2',7'-dichlorofluorescein diacetate) after treatment of the cells with complex (**1**) (2 × IC_{50} of 24 h) for 4h. The H_2O_2 was used as a positive control. Moreover, the free Lap was analyzed. Fluorescence measurements were carried out to analyze the intracellular ROS generation. The green fluorescence observed indicate the formation of ROS in the analyzed cells, but a stronger effect was observed in the cells treated with complex (**1**) (Figure 7). Thus, complex (**1**) can disturb the cellular redox and the ROS generated can lead the cell death by apoptosis.

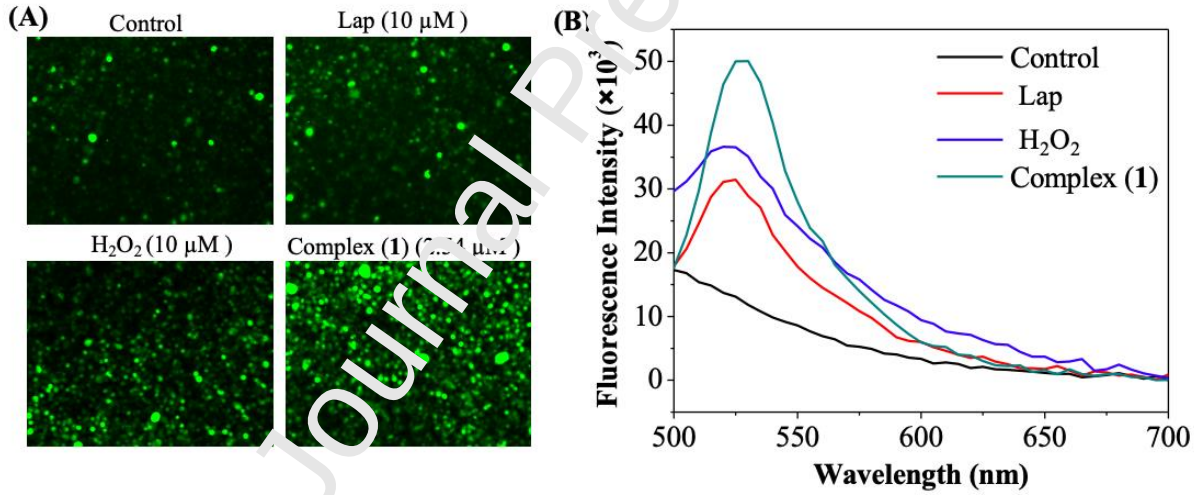

Figure 7. Effects of complex (**1**) on ROS generation in MDA-MB-231 cells. (**A**) Representative pictures of ROS generation in MDA-MB-231 cells after treatment with H_2O_2 (10 µM), Lap (10 µM) and complex (**1**) (2.54 µM), detected by H_2DCFDA staining and (**B**) Fluorescence signal detected for the cells in the presence of the compounds.

DNA-interaction studies

Modification in the DNA structure may result in conformational changes that can modify and affect the message of the genetic sequence. Thus, irreversible alterations can influence the development of tumor cells, and induce cell death. One of the ways reported for the action of cisplatin is the ability of binding to the N7 of guanine of DNA, and blocking cell

division, causing cell death. Therefore, DNA is an exploring target when it comes to developing drugs to treat cancer[55,56].

The interaction of ruthenium complexes (**1**) and (**2**) with DNA was investigated by circular dichroism, analysis of DNA mobility and competitive DNA fluorescence studies. Each of these techniques provides information about the type of interaction that occurs between the ruthenium complexes and the DNA molecule.

DNA shows two bands in the circular dichroism (CD) spectra, a positive band at 275 nm and a negative band at 245 nm, due to the base stacking interaction and right-handed helicity, respectively. Compounds that can interact with DNA may cause conformational changes at the CD spectra. The interaction of ruthenium complexes with DNA was monitored by incubating different molar ratios of complexes and CT-DNA. The complex (**1**) demonstrated a weak interaction with DNA, given no significant changes were observed in the intensity of the ellipticity of CT-DNA spectra (Figure 8A). This result indicates that complex (**1**) cannot make significant conformational changes in the CT-DNA structure.

In order to gain more insight into the nature of the interactions between ruthenium complexes and DNA, the gel electrophoresis of pBR322 was performed to investigate the influence of complexes on the mobility of this plasmid. The pBR322 showed three different bands related with the shapes of the DNA, a band namely supercoiled form (SC), circular form (OC) and the linear form (L) (Figure 8B). The intensity of the bands decreases (or even disappeared) when the concentration of the ruthenium complex (**1**) increased (Figure 8B, lines a, b and c). These results suggest that the ruthenium complex (**1**) interacts with DNA covalently or by minor groove, promoting the expulsion of ethidium bromide from the DNA structure, preventing the visualization of the bands.

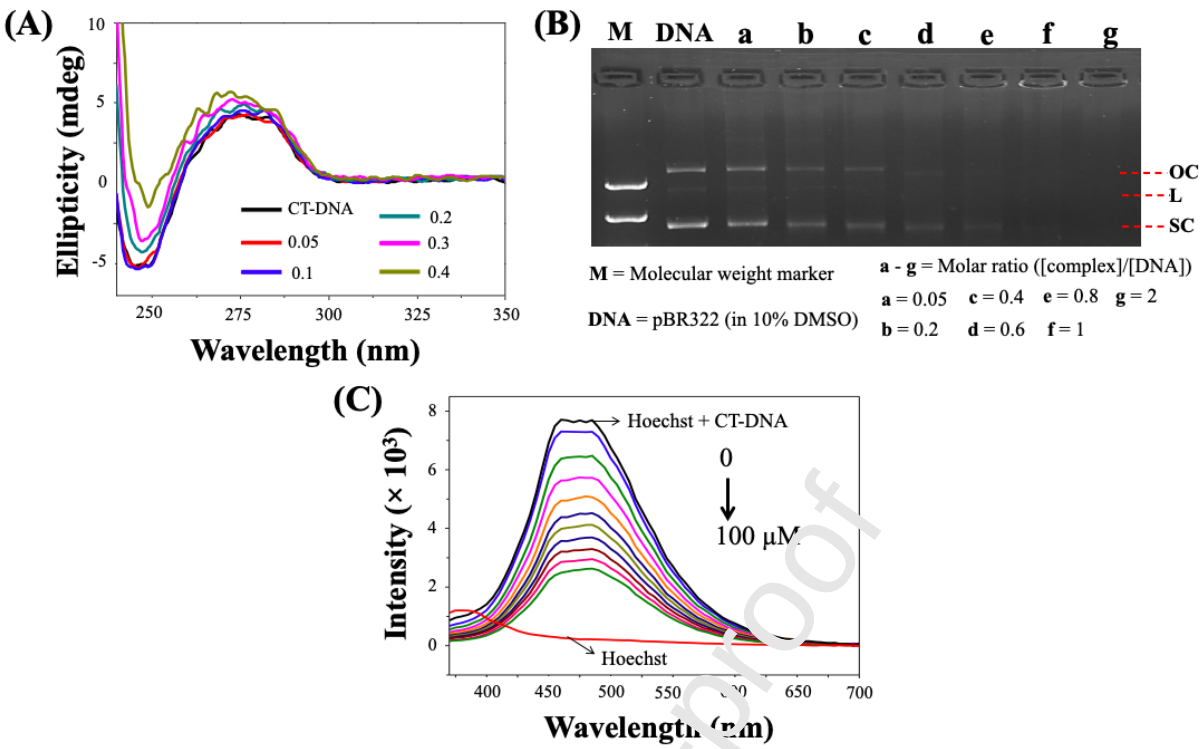

Figure 8. Interaction of complex (**1**) with DNA molecule. (**A**) Circular dichroism spectra of CT-DNA incubated with complex (**1**) at different molar ratios (Ri) = [complex]/[CT-DNA] = 0.05, 0.1, 0.2, 0.3 and 0.4, (**B**) Agarose gel electrophoresis image of pBR322 plasmid DNA incubated for 18 h at 37 °C with complex (**1**). Lane 1 (M): molecular weight marker, lane 2 (DNA): pure pBR322 with DMSO, lane 3 - 9 (a - g) = Ri = 0.05 to 2 and (**C**) Emission spectra of Hoechst–CT-DNA (2.7 µM; 125 µM) in the absence and presence of increasing amounts of complex (**1**) (0 – 100 µM).

To further investigate whether the complex (**1**) may be covalently interacting with DNA, a solution of complex (**1**) was prepared with guanosine, and monitoring was carried out by $^{31}P\{^{1}H\}$ NMR. The $^{31}P\{^{1}H\}$ NMR spectra (Fig. S15) showed no alteration of signals of complex (**1**), indicating that it is not able to form a strong association with the DNA structure, then rejecting the possibility of covalent interaction.

To confirm the hypothesis of interaction by minor groove, a competitive binding study with Hoechst 33258 was used. This fluorophore is able to interact with DNA by a minor groove and the formed Hoechst-DNA adduct emits a high fluorescence at 450 nm, when excited at 343 nm. If the compounds interact with the DNA through the minor grooves, it will

compete with Hoechst, replacing it from the DNA structure and so, the fluorescence intensity will decrease[57]. A considerable decrease in fluorescence intensity of Hoechst-DNA adduct was performed detected after increases in the ruthenium complex (**1**) concentration (Figure 8C). Overall, these results indicate that complexes (**1**) and (**2**) interact with the DNA by minor grooves. Previous research findings showed the same behavior for ruthenium complexes containing lawsone as ligand, as well as for ruthenium-arene complexes[25,58,59].

Protein binding studies

Albumin is the protein responsible for transporting endogenous and exogenous substances, such as anticancer drugs, through the body. Thus, when it comes to drug development, the investigators have been studying the interaction of the drug candidates with the albumin, because this protein may be the carrier of the drug[60,61].

Bovine serum albumin (BSA) is structurally homologous with Human Serum Albumin (HSA), and for that reason, is extensively used as the model protein binding studies. BSA exhibits intrinsic fluorescence mainly due to the presence of tryptophan residue. The fluorescence of BSA provides significant information about the structure, dynamics and protein folding, thus any change in the fluorescence will indicate changes in its structure. Fluorescence quenching is related to the process that causes a decrease in the fluorescence intensity after the incubation with a fluorophore (ruthenium complexes, in this case)[36].

The BSA-binding experiment was performed by incubating the BSA with ruthenium complexes (**1**) and (**2**) in different concentrations, at 298 and 310 K, monitoring the fluorescence intensity. Complexes (**1**) and (**2**) acted as quenchers since successive increases of complexes concentration promoted decreases in the intensity of BSA fluorescence (Figure 9A), evidencing that the complexes interact with the BSA, changing its structure. The interactions can occur by static or dynamic mechanism, or a combination of both. To distinguish these mechanisms, the fluorescence quenching was studied at different temperatures, and analyzed by the Stern-Volmer constant (K_{sv}) showing its increase as the

temperatures rise (Table 2). Dynamic quenching occurs when the fluorophore and the quencher (ruthenium complexes) come into contact with the transient excited state, and static quenching, indicating the formation of fluorophore-quencher complexes in the ground state. Thus, the increase in the temperature favors dynamic quenching, because this mechanism depends on the diffusion, therefore high temperatures result in high diffusion coefficient, and consequently, the K_{sv} constant must increase when the temperature rises. On the other hand, static quenching is disadvantaged with the increase in temperature, resulting in a low value of K_{sv} constant[36,62]. Therefore, as the K_{sv} values increase with the temperature, the dynamic mechanism may be involved. On the other hand, the k_q values obtained are higher than the pure dynamic quenching ($k_q = 2.0 \times 10^{10}$ M^{-1} s^{-1}), indicating that the interaction between ruthenium complexes (**1**) and (**2**) with BSA occurs by both a dynamic and static quenching mechanism.

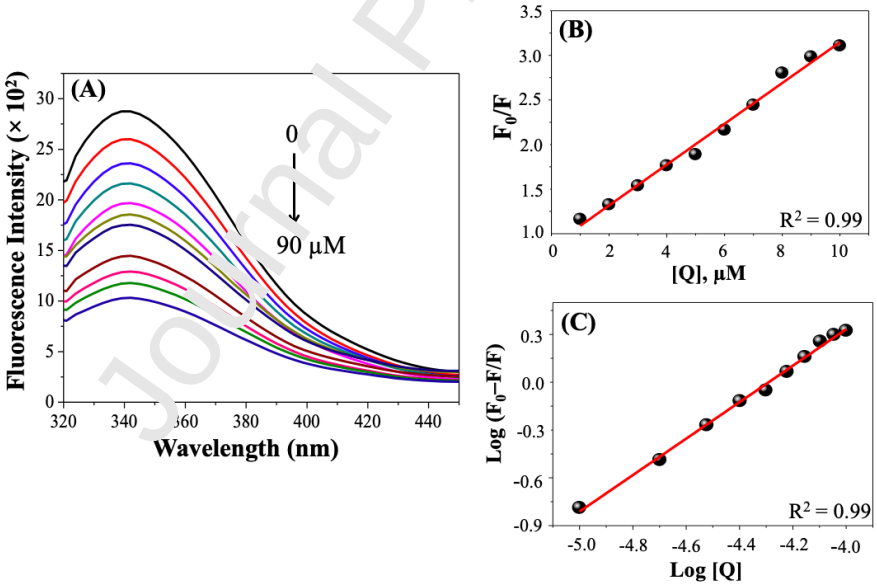

Figure 9. Interaction of complex (**1**) with BSA. (**A**) Fluorescence spectra of BSA (2.5 µM) in the absence and presence of increasing concentrations of complex (**1**), (**B**) Stern-Volmer and (**C**) $\log(F_0\text{-}F/F)$ $_{vs}$. $\log[Q]$ plots, at 310 K.

The values of the binding constant (K_b) and number of binding sites (*n*), listed in Table 2, reveals that the complexes show a moderate interaction with BSA, where K_b values

compare to other ruthenium complexes found in the literature[58,63,64]. The *n* values found were approximately 1, indicating that the interaction involves one site in the protein.

Table 2. The values of K_{sv} (M^{-1}), k_q (M^{-1} s^{-1}), K_b (M^{-1}) and *n* for interaction of BSA and complexes (**1**) and (**2**)

Complexes	T (K)	K_{sv} (10^4)	k_q (10^{12})	K_b (10^4)	*n*
1	298	2.21± 0.24	2.21	8.55 ± 0.38	1.16
	310	2.28 ± 0.14	2.28	9.33 ± 0.83	1.15
2	298	2.15 ± 0.10	2.15	2.27 ± 0.37	1.18
	310	2.34 ± 0.11	2.34	2.41 ± 0.20	1.07

To gain further insight regarding the type of force involved in the interaction between the ruthenium complexes and BSA, some thermodynamic parameters were determined (enthalpy change, entropy change, and Gibbs free energy change). Table 3 presents the thermodynamic parameters for the system analyzed. The positive values of enthalpy and entropy changes indicate the involvement of hydrophobic interactions between BSA and complexes (**1**) and (**2**). Furthermore, the negative values of Gibbs free energy suggest that this interaction is spontaneous[65].

Table 3. Thermodynamic parameters for interaction of BSA and complexes (**1**) and (**2**)

Complexes	T(K)	ΔG° (kJ mol^{-1})	ΔH° (kJ mol^{-1})	ΔS° (J mol^{-1} K^{-1})
1	298	–28.13	5.58	113.12
	310	–29.49		113.13
2	298	–24.99	3.83	96.71
	310	–25.85		95.74

Conclusions

In this paper, two new ruthenium(II) complexes containing diphosphine (dppm = *bis*(diphenylphosphine)methane, (**1**) Lapachol and (**2**) Lawsone as ligands were synthesized and fully characterized by elemental analyses, molar conductivity, UV-Vis, IR, $^{31}P\{^1H\}$, ^1H

and ^{13}C NMR. Crystal structure determination was possible for complex (**1**), confirming the proposed composition. Complex (**1**) showed a 20-fold higher activity to the triple-negative breast cancer (MDA-MB-231) when compared to non-tumor breast (MCF-10A). Moreover, complex (**1**) showed the ability to inhibit cell migration and colony formation and to induce cell cycle arrest and apoptosis by activating the mitochondrial apoptosis pathway through ROS induction and loss of mitochondrial membrane potential ($\Delta\Psi m$) in MDA-MB-231 cells. DNA binding studies suggest that complexes (**1**) and (**2**) interact with DNA by minor grooves. The interactions with BSA occurs by dynamic and static mechanism in a spontaneous process with the involvement of hydrophobic interactions. On the basis of the reported results, the ruthenium(II)/diphosphine-naphthoquinone can be further studied using *in vivo* models, as they represent promising candidates for anticancer applications.

Conflicts of interest

There are no conflicts to declare.

Acknowledgements

The authors are grateful for the financial support provided by the Brazilian Agencies of Research: CAPES, CNPq and FAPESP. K. M. Oliveira would like to thank FAPESP for a research fellowship (grant number 2014/04147-9), and Alzir A. Batista for a research grant (2016/16312-0). R. S. Corrêa would like to thank CNPq for the financial support (project 403588/2016-2 and 308370/2017-1). We would like to thank Dr. Eduardo Ernesto Castellano from IFSC-USP who provided the X-ray diffractometer for the crystallographic measurements.

References

[1] C.C. Konkankit, S.C. Marker, K.M. Knopf, J.J. Wilson, Anticancer activity of complexes of the third row transition metals, rhenium, osmium, and iridium, Dalt. Trans. 47 (2018) 9934–9974.

[2] B. Rosenberg, Platinum Complexes for the Treatment of Cancer, Interdiscip. Sci. Rev. 3 (1978) 134–147.

[3] B. Rosenberg, L. Van Camp, J.E. Trosko, V.H. Mansour, Platinum compounds: a new class of potent antitumour agents, Nature. 222 (1969) 385–386.

[4] J. Zhao, S. Li, X. Wang, G. Xu, S. Gou, Dinuclear Organoruthenium Complexes

Exhibiting Antiproliferative Activity through DNA Damage and a Reactive-Oxygen-Species-Mediated Endoplasmic Reticulum Stress Pathway, Inorg. Chem. 58 (2019) 2208–2217.
[5] R.G. Kenny, C.J. Marmion, Toward Multi-Targeted Platinum and Ruthenium Drugs—A New Paradigm in Cancer Drug Treatment Regimens?, Chem. Rev. 119 (2019) 1058–1137.
[6] M.A. Jakupec, M. Galanski, V.B. Arion, C.G. Hartinger, B.K. Keppler, Antitumour metal compounds: more than theme and variations, Dalt. Trans. (2008) 183–194.
[7] S.M. Meier-Menches, C. Gerner, W. Berger, C.G. Hartinger, B.K. Keppler, Structure–activity relationships for ruthenium and osmium anticancer agents – towards clinical development, Chem. Soc. Rev. 47 (2018) 909–928.
[8] S. Thota, D.A. Rodrigues, D.C. Crans, E.J. Barreiro, Ru (II) Compounds : Next-Generation Anticancer Metallotherapeutics ?, J. Med. Chem. 61 (2018) 5805–5821.
[9] A. Levina, A. Mitra, P.A. Lay, Recent developments in ruthenium anticancer drugs, Metallomics. 1 (2009) 458–470.
[10] F.E. Poynton, S.A. Bright, S. Blasco, D.C. Williams, J.M. Kelly, T. Gunnlaugsson, The development of ruthenium(II) polypyridyl complexes and conjugates for in vitro cellular and in vivo applications, Chem. Soc. Rev. 46 (2017) 7706–7756.
[11] C.G. Hartinger, P.J. Dyson, Bioorganometallic chemistry—from teaching paradigms to medicinal applications, Chem. Soc. Rev. 38 (2009) 391–401.
[12] A. Rilak Simović, R. Masnikosa, I. Bratsos, E. Alessio, Chemistry and reactivity of ruthenium(II) complexes: DNA/protein binding mode and anticancer activity are related to the complex structure, Coord. Chem. Rev. 398 (2019) 113011.
[13] M. Abid, F.S. and A. Azam, Ruthenium Complexes: An Emerging Ground to the Development of Metallopharmaceuticals for Cancer Therapy, Mini-Reviews Med. Chem. 16 (2016) 772–786.
[14] D.A. Smithen, H. Yin, M.H.R. Beh, M. Hetu, T.S. Cameron, S.A. McFarland, A. Thompson, Synthesis and Photobiological Activity of Ru(II) Dyads Derived from Pyrrole-2-carboxylate Thioamides, Inorg. Chem. 56 (2017) 4121–4132.
[15] E. Alessio, L. Messori, NAMI-A and KP1019/1339, Two Iconic Ruthenium Anticancer Drug Candidates Face-to-Face: A Case Story in Medicinal Inorganic Chemistry, Molecules. 24 (2019) 1995.
[16] E. Alessio, Thirty Years of the Drug Candidate NAMI-A and the Myths in the Field of Ruthenium Anticancer Compounds: A Personal Perspective, Eur. J. Inorg. Chem. 2017 (2017) 1549–1560.
[17] R. Trondl, P. Heffeter, C.R. Kowol, M.A. Jakupec, W. Berger, B.K. Keppler, NKP-1339, the first ruthenium-based anticancer drug on the edge to clinical application, Chem. Sci. 5 (2014) 2925–2932.
[18] P. Chellan, P.J. Sadler, Enhancing the Activity of Drugs by Conjugation to Organometallic Fragments, Chem. Eur. J. 26 (2020) 8676.
[19] F. Qu, S. Park, K. Martinez, J.L. Gray, F.S. Thowfeik, J.A. Lundeen, A.E. Kuhn, D.J. Charboneau, D.L. Gerlach, M.M. Lockart, J.A. Law, K.L. Jernigan, N. Chambers, M. Zeller, N.A. Piro, W.S. Kassel, R.H. Schmehl, J.J. Paul, E.J. Merino, Y. Kim, E.T. Papish, Ruthenium Complexes are pH-Activated Metallo Prodrugs (pHAMPs) with Light-Triggered Selective Toxicity Toward Cancer Cells, Inorg. Chem. 56 (2017) 7519–7532.
[20] S. Monro, K.L. Colón, H. Yin, J. Roque, P. Konda, S. Gujar, R.P. Thummel, L. Lilge, C.G. Cameron, S.A. McFarland, Transition Metal Complexes and Photodynamic Therapy from a Tumor-Centered Approach: Challenges, Opportunities, and Highlights from the Development of TLD1433, Chem. Rev. 119 (2019) 797–828.

[21] K.M. Oliveira, R.S. Corrêa, M.I.F. Barbosa, J. Ellena, M.R. Cominetti, A.A. Batista, Ruthenium(II)/triphenylphosphine complexes: An effective way to improve the cytotoxicity of lapachol, Polyhedron. 130 (2017) 108–114.
[22] K.M. Oliveira, L.-D. Liany, R.S. Corrêa, V.M. Deflon, M.R. Cominetti, A.A. Batista, Selective Ru(II)/lawsone complexes inhibiting tumor cell growth by apoptosis, J. Inorg. Biochem. 176 (2017) 66–76.
[23] K. Oliveira, E.J. Peterson, M. Carroccia, M.R. Cominetti, V.M. Deflon, N.P. Farrell, A.A. Batista, R.S. Correa, Ru(II)-naphthoquinone complexes with high selectivity for triple negative breast cancer, Dalt. Trans. (2020). doi:10.1039/D0DT01091J.
[24] A.E. Graminha, J. Honorato, L.L. Dulcey, L.R. Godoy, M.F. Barbosa, M.R. Cominetti, A.C. Menezes, A.A. Batista, Evaluation of the biological potential of ruthenium(II) complexes with cinnamic acid, J. Inorg. Biochem. 206 (2020) 111021.
[25] R.A. De Grandis, P.W. da S. dos Santos, K.M. de Oliveira, A.R.T. Machado, A.F. Aissa, A.A. Batista, L.M.G. Antunes, F.R. Pavan, Novel lawsone-containing ruthenium(II) complexes: Synthesis, characterization and anticancer activity on 2D and 3D spheroid models of prostate cancer cells, Bioorg. Chem. 85 (2019) 455–468.
[26] M.A. Naves, A.E. Graminha, L.C. Vegas, L. Luna-Dulcey, J. Honorato, A.C.S. Menezes, A.A. Batista, M.R. Cominetti, Transport of the Ruthenium Complex [Ru(GA)(dppe)2]PF6 into Triple-Negative Breast Cancer Cells Is Facilitated by Transferrin Receptors, Mol. Pharm. 16 (2019) 1167–1183.
[27] L.-J. Huang, F.-C. Chang, K.-H. Lee, J.-P. Wang, C.-M. Teng, S.-C. Kuo, Synthesis and antiplatelet, antiinflammatory, and antiallergic activities of substituted 3-chloro-5,8-dimethoxy-1,4-naphthoquinone and related compounds, Bioorg. Med. Chem. 6 (1998) 2261–2269.
[28] K.W. Wellington, Understanding cancer and the anticancer activities of naphthoquinones – a review, RSC Adv. 5 (2015) 20309–20338.
[29] M. Kubanik, W. Kandioller, K. Kim, R.F. Anderson, E. Klapproth, M.A. Jakupec, A. Roller, T. Söhnel, B.K. Keppler, C.G. Hartinger, Towards targeting anticancer drugs: ruthenium(II)–arene complexes with biologically active naphthoquinone-derived ligand systems, Dalt. Trans. 45 (2016) 13091–13103.
[30] M.B.P. Moreira, D. R. M.; de Sá, M. S.; Macedo, T. S.; Reys, J. R. M.; Santana, A. E. G.; Silva, T. L.; Maia, G. L. A.; Barbosa-Filho, J. M.; Camara, C. A.; Silva, T. M. S.; Silva, K. N.; Guimarães, E. T.; Santos, R. R.; Goulart, M. O. F.; Soares, Evaluation of Naphthoquinones Identified the Acetylated Isolapachol as a Potent and Selective Antiplasmodium Agent, J Enzym. Inhib Chem. 30 (2014) 615–621.
[31] B.P. Sullivan, T.J. Meyer, Comparisons of the Physical and Chemical Properties of Isomeric Pairs. 2. Photochemical, Thermal, and Electrochemical Cis-Trans Isomerizations of M(Ph2PCH2PPh2)2Cl2 (M = RuII, OsII), Inorg. Chem. 21 (1982) 1037–1040.
[32] S. Complexes, S. Complexes, T. Phosphines, Some Complexes of Tertiary Phosphines with Ruthenium(II) and Osmium(II), Proc. Chem. Soc. 153 (1960) 896–904.
[33] CrysAlis Pro and CrysAlis RED, (2015). https://www.rigaku.com/products/smc/crysalis.
[34] G.M. Sheldrick, Crystal structure refinement with SHELXL, Acta Crystallogr. Sect. C Struct. Chem. 71 (2015) 3–8.
[35] C.F. Macrae, I. Sovago, S.J. Cottrell, P.T.A. Galek, P. McCabe, E. Pidcock, M. Platings, G.P. Shields, J.S. Stevens, M. Towler, P.A. Wood, Mercury 4.0: from visualization to analysis, design and prediction, J. Appl. Crystallogr. 53 (2020) 226–235.
[36] J.R. Lacowicz, Principles of Fluorescence Spectroscopy, Kluver Academic/Plenum

Publishers, New York, 1999.
[37] M. Ganeshpandian, R. Loganathan, E. Suresh, A. Riyasdeen, M.A. Akbarsha, M. Palaniandavar, New ruthenium(ii) arene complexes of anthracenyl-appended diazacycloalkanes: effect of ligand intercalation and hydrophobicity on DNA and protein binding and cleavage and cytotoxicity., Dalton Trans. 43 (2014) 1203–19.
[38] T. Mosmann, Rapid colorimetric assay for cellular growth and survival: Application to proliferation and cytotoxicity assays, J. Immunol. Methods. 65 (1983) 55–63.
[39] K. Nakamoto, Infrared and Raman Spectra of Inorganic and Coordination Compounds, 6ª edição, 2009.
[40] V.S. Velozo-Sá, L.R. Pereira, A.P. Lima, F. Mello-Andrade, M.R.M. Rezende, R.M. Goveia, W.C. Pires, M.M. Silva, K.M. Oliveira, A.G. Ferreira, J. Ellena, V.M. Deflon, C.K. Grisolia, A.A. Batista, E.P. Silveira-Lacerda, In vitro cytotoxicity and in vivo zebrafish toxicity evaluation of Ru(II)/2-mercaptopyrimidine complexes, Dalt. Trans. 48 (2019) 6026–6039.
[41] M.I.F. Barbosa, R.S. Corrêa, K.M. De Oliveira, C. Rodrigues, J. Ellena, O.R. Nascimento, V.P.C. Rocha, F.R. Nonato, T.S. Macedo, J.M. Barbosa-Filho, M.B.P. Soares, A.A. Batista, Antiparasitic activities of novel ruthenium/lapachol complexes, J. Inorg. Biochem. 136 (2014) 33–39.
[42] J.C.S. Lopes, J.L. Damasceno, P.F. Oliveira, D.C. Tavares, V.M. Deflon, N.P. Lopes, M. Pivatto, A.A. Batista, P.I.S. Maia, G. Von Poelhsitz, Ruthenium(II) Complexes Containing Anti-Inflammatory Drugs as Ligands: Synthesis, Characterization and in vitro Cytotoxicity Activities on Cancer Cell Lines, J. Brazilian Chem. Soc. 26 (2015) 1838–1847.
[43] I.K. Larsen, L.A. Andersen, B.F. Pedersen, Structures of two crystalline modifications of lapachol, Acta Crystallogr. Sect. C. 48 (1992) 2009–2013.
[44] R.S. Correa, L.M. Bomfim, K.M. Oliveira, D.R.M. Moreira, M.B.P. Soares, J. Ellena, D.P. Bezerra, A.A. Batista, Ru(II) complexes containing uracil nucleobase analogs with cytotoxicity against tumor cells, J. Inorg. Biochem. 198 (2019) 110751.
[45] R.S. Correa, V. Freire, M.I.F. Barbosa, D.P. Bezerra, L.M. Bomfim, D.R.M. Moreira, M.B.P. Soares, J. Ellena, A.A. Batista, Ru(II)–thyminate complexes: new metallodrug candidates against tumor cells, New J. Chem. 42 (2018) 6794–6802.
[46] R.S. Corrêa, J.P. Barolin, M.I.F. Barbosa, J. Ellena, A.A. Batista, The effect of guest molecules on the conformation and molecular assembly of the fac-[RuCl3(NO)(dppb)] complex, J. Mol. Struct. 1048 (2013) 11–17.
[47] P. Mehlen, A. Puisieux, Metastasis: A question of life or death, Nat. Rev. Cancer. 6 (2006) 449–458.
[48] X. Huang, H.D. Halicka, F. Traganos, T. Tanaka, A. Kurose, Z. Darzynkiewicz, Cytometric assessment of DNA damage in relation to cell cycle phase and apoptosis, Cell Prolif. 38 (2005) 223–243.
[49] J. Li, H. Chen, L. Zeng, T.W. Rees, K. Xiong, Y. Chen, L. Ji, H. Chao, Mitochondria-targeting cyclometalated iridium(III) complexes for tumor hypoxic imaging and therapy, Inorg. Chem. Front. 6 (2019) 1003–1010.
[50] S. Wen, D. Zhu, P. Huang, Targeting cancer cell mitochondria as a therapeutic approach, Future Med. Chem. 5 (2013) 53–67.
[51] S. Sakamuru, X. Li, M.S. Attene-Ramos, R. Huang, J. Lu, L. Shou, M. Shen, R.R. Tice, C.P. Austin, M. Xia, Application of a homogenous membrane potential assay to assess mitochondrial function., Physiol. Genomics. 44 (2012) 495–503.
[52] A.T. Dharmaraja, Role of Reactive Oxygen Species (ROS) in Therapeutics and Drug Resistance in Cancer and Bacteria, J. Med. Chem. 60 (2017) 3221–3240.
[53] L. Zeng, Y. Chen, J. Liu, H. Huang, R. Guan, L. Ji, H. Chao, Ruthenium(II)

Complexes with 2-Phenylimidazo[4,5-f][1,10]phenanthroline Derivatives that Strongly Combat Cisplatin-Resistant Tumor Cells, Sci Rep. 6 (2016) 19449.
[54] L.-N. Li, L. Wang, Y.-N. Cheng, Z.-Q. Cao, X.-K. Zhang, X.-L. Guo, Discovery and Characterization of 4-Hydroxy-2-pyridone Derivative Sambutoxin as a Potent and Promising Anticancer Drug Candidate: Activity and Molecular Mechanism, Mol. Pharm. 15 (2018) 4898–4911.
[55] D. Shaloam, P.B. Tchounwou, Cisplatin in cancer therapy: Molecular mechanisms of action, Eur. J. Pharmacol. 740 (2014) 364–378.
[56] A. Kellett, Z. Molphy, C. Slator, V. McKee, N.P. Farrell, Molecular methods for assessment of non-covalent metallodrug–DNA interactions, Chem. Soc. Rev. 48 (2019) 971–988.
[57] N. Narayanaswamy, M. Kumar, S. Das, R. Sharma, P.K. Samanta, S.K. Pati, S.K. Dhar, T.K. Kundu, T. Govindaraju, A thiazole coumarin (TC) turn-on fluorescence probe for AT-base pair detection and multipurpose applications in different biological systems, Sci. Rep. 4 (2014) 1–10.
[58] B.N. Cunha, L. Colina-Vegas, A.M. Plutín, R.G. Silveira, J. Honorato, K.M. Oliveira, M.R. Cominetti, A.G. Ferreira, E.E. Castellano, A.A. Batista, Hydrolysis reaction promotes changes in coordination mode of Ru(II)/acylthiourea organometallic complexes with cytotoxicity against human lung tumor cell lines, J. Inorg. Biochem. 186 (2018) 147–156.
[59] L. Colina-Vegas, K.M. Oliveira, B.N. Cunha, M.R. Cominetti, M. Navarro, A. Azevedo Batista, Anti-Proliferative and Anti-Migration Activity of Arene–Ruthenium(II) Complexes with Azole Therapeutic Agents, Inorganics. 6 (2018) 132.
[60] W. Ma, Z. Tian, S. Zhang, X. He, J. Li, Z. Xia, X. Chen, Z. Liu, Lysosome targeted drugs: rhodamine B modified N^N-chelating ligands for half-sandwich iridium(iii) anticancer complexes, Inorg. Chem. Front. 5 (2018) 2587–2597.
[61] J.J. Miller, L.M.F. Gomes, T. Storr, A. Casini, The Interaction of Metal Compounds with Protein Targets: New Tools in Medicinal Chemistry and Chemical Biology, Encycl. Inorg. Bioinorg. Chem. (2017).
[62] Y. Shu, M. Liu, S. Chen, X. Chen, J. Wang, New Insight into Molecular Interactions of Imidazolium Ionic Liquids with Bovine Serum Albumin, J. Phys. Chem. B. 115 (2011) 12306–12314.
[63] R.S. Correa, K.M. De Oliveira, F.G. Delolo, A. Alvarez, R. Mocelo, A.M. Plutin, M.R. Cominetti, E.E. Castellano, A.A. Batista, Ru(II)-based complexes with N-(acyl)-N',N'-(disubstituted)thiourea ligands: Synthesis, characterization, BSA- and DNA-binding studies of new cytotoxic agents against lung and prostate tumour cells, J. Inorg. Biochem. 150 (2015) 63–71.
[64] P. Mandal, B.K. Kundu, K. Vyas, V. Sabu, A. Helen, S.S. Dhankhar, C.M. Nagaraja, D. Bhattacherjee, K.P. Bhabak, S. Mukhopadhyay, Ruthenium(II) arene NSAID complexes: inhibition of cyclooxygenase and antiproliferative activity against cancer cell lines, Dalt. Trans. 47 (2018) 517–527.
[65] P.D. Ross, S. Subramanian, Thermodynamics of protein association reactions: forces contributing to stability., Biochemistry. 20 (1981) 3096–3102.

Synopsis

The naphthoquinones Lapachol and Lawsone can form new ruthenium compounds with promising anticancer properties.

Declaration of Interest Statement

There are no conflicts to declare.

Highlights

- Ruthenium-naphthoquinone compounds with promising anticancer properties.
- Promising cytotoxicity against breast, lung and prostate cancer cells.
- Exciting results of selectivity are reported against breast cancer cells.
- Complex inhibits cell migration and colony formation of breast cancer cells.
- Complex induces apoptosis by activation of the mitochondrial pathway.